JOINT INSTITUTE FOR NUCLEAR RESEARCH

Dzhelepov Laboratory of nuclear problems

FINAL REPORT ON THE START PROGRAMME

"*Radiation protection and the safety of radiation sources*"

Supervisor:

Prof. Dr. S. Abdelshakour

Joint Institute for Nuclear Research

Student:

Hagar Hassanin Ibrahim

The British University in Egypt (BUE)

Participation period:

May 12 – June 22

Winter Session 2024

Dubna, 2024

Table of Contents

List of Figures

Abstract

This study investigates how to improve gamma-ray detection with a variety of cutting-edge detectors, with an emphasis on radiation safety in medical imaging. The investigation uses pixel detectors to measure alpha radiation, Bismuth Germanate (BGO) and Lanthanum Bromide ($LaBr_3$) scintillator detectors, and Cadmium Telluride (CdTe) detectors for calibration. Furthermore, to quantify intensity fluctuations, we theoretically calculated the X-ray attenuation coefficients for various human body tissues, such as tumors, fat, and muscle. The distance between graphite atoms at different energies was measured using a monochromator, which produced precise spectra for each experiment. Our results show that applying a higher voltage to $LaBr_3$ detectors improves their performance by boosting resolution, especially for Co-60 gamma emissions. This study emphasizes how important it is for sophisticated detection systems to maximize medical imaging and reduce undesired radiation exposure to increase patient safety and diagnostic accuracy. This work done by using monte Carlo simulation, ROOT software and Python.

Introduction

Radiation is a form of energy that travels through space and can penetrate various materials. It can be broadly categorized into two main types: ionizing and non-ionizing radiation. It plays a crucial role in numerous fields, including medicine, industry, and scientific research. There are two types, the first is ionizing radiation has enough energy to remove tightly bound electrons from atoms, creating ions. This type of radiation can alter chemical bonds and damage living tissue. This form of radiation such as alpha, Beta, Gamma rays, x-rays and neutrons. While the non-ionizing radiation lacks the energy to ionize atoms or molecules. It generally causes excitation or heating effects rather than ionization. Such as ultraviolet (UV) Radiation, radio waves, visible light and infrared radiation.

Understanding the different types of radiation and their applications is essential for harnessing their benefits while minimizing potential risks. Radiation has a wide range of applications across different fields, significantly impacting modern life. For instance, using radiation in medical applications such as X-ray, CT scans, and PET scans using ionizing radiation to create detailed images aiding in diagnosis and treatment. Furthermore, radiation therapy uses ionizing radiation to destroy cancerous cells while sparing surrounding healthy tissue. However, the use of ionizing radiation comes with inherent risks, including potential harm to healthy tissues and an increased risk of cancer with prolonged or excessive exposure. Therefore, radiation protection is a critical aspect of medical practice, aiming to minimize these risks while maximizing the benefits of medical imaging and therapy. Radiation protection is a critical aspect of medical imaging, especially in the context of diagnosing and treating tumors within the human body. As medical imaging technologies advance, the ability to detect and monitor tumors with higher precision and lower risk to patients becomes increasingly important. This research focuses on enhancing radiation protection through the application of various detectors and measurement techniques, with a specific emphasis on tumor imaging and analysis. Radiation protection involves the implementation of safety measures and protocols to reduce unnecessary exposure to both patients and healthcare workers. This includes optimizing imaging techniques, using protective equipment, and adhering to established guidelines and regulations. The primary goals are to achieve the desired medical outcomes with the lowest possible radiation dose and to prevent stochastic effects, such as cancer, and deterministic effects, such as tissue damage. Advancements in scientific tools and technologies have significantly contributed to improving radiation protection in the medical field. Radiation, with its diverse forms and applications, is a powerful tool that drives advancements in medicine, industry, research, and beyond.

Understanding its types and uses is essential for maximizing its benefits while implementing appropriate safety measures to mitigate risks. This knowledge forms the foundation for ongoing innovations and improvements in numerous fields, enhancing our quality of life and expanding our scientific horizons.

Detectors are used to identify and measure various properties of nuclear radiation. Their primary purpose is to measure energy, position, timing, and sometimes the identity of the particles. There are many types of detectors such as semiconductor detectors, Scintillators detectors and gas filled detectors. For instance, the development of sophisticated semiconductor detectors, such as Cadmium Telluride (CdTe) detectors, has enhanced the accuracy and efficiency of radiation measurements. CdTe detectors are known for their high resolution and sensitivity, making them invaluable in calibrating and monitoring radiation doses. Scintillator detectors, such as Bismuth Germanate (BGO) and Lanthanum Bromide (LaBr), have also advanced radiation protection. These detectors are used to convert radiation into visible light, which is then measured to determine radiation levels. Their high density and effective scintillation properties make them ideal for medical imaging applications, where precise localization and imaging of tumors are crucial. Pixel detectors represent another leap forward in radiation detection technology. These detectors are particularly effective in detecting alpha particles, providing detailed imaging at the cellular level. This capability is essential for identifying and analyzing the early stages of tumor development, allowing for timely and targeted interventions.

1. Semiconductor detectors

Cadmium Telluride (CdTe) Detector

The X-123-CdTe detector is recommended for higher energy X-rays above 30 keV or so. It has an interface, a power supply, an x-ray and gamma-ray detector, a preamplifier digital pulse processor, and more. It can be applied to radiology, mammography, and the detection of uranium and plutonium. The CdTe detector is about 100% efficient for all characteristic X-rays up to 100 keV, while the other detectors' 0.5 mm silicon loses sensitivity above 15 keV. In addition to XRF for rare earth metals, lead, mercury, and other higher Z materials, it is frequently employed in the characterization of X-ray tubes.

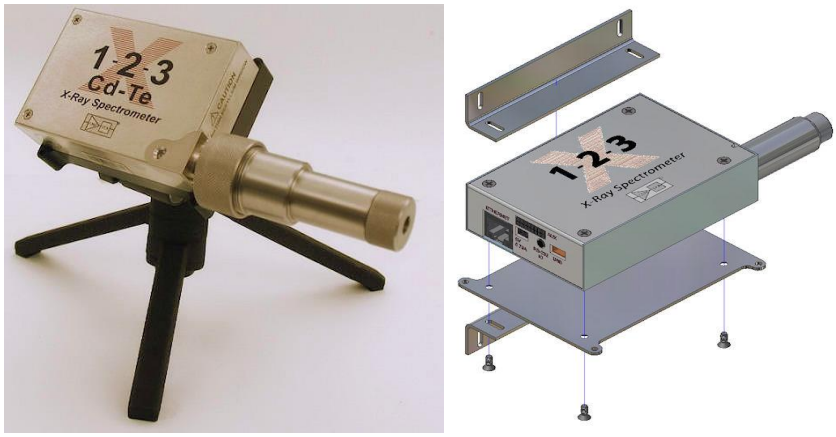

Fig. 1 CdTe Detector

The detector is connected to a specially designed charge-sensitive preamplifier and installed atop a thermoelectric cooler together with the input FET. The detector and preamplifier's electrical noise is reduced by the thermoelectric cooler, yet the cooling process is transparent to the user and functions like a system at room temperature. Using a unique feedback mechanism, the charge-sensitive preamplifier injects reset pulses into the detector through the high voltage connection. Performance is not compromised by the X-123's small size. The range of 145 eV FWHM to 260 eV FWHM is the resolution for the 5.9 keV peak of 55Fe, contingent on the type of detector and shaping time constant.

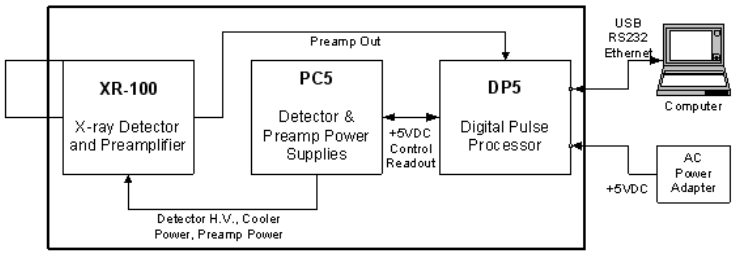

Fig. 2 X-123 Architecture and Connection Diagram

Energy Calibration Using CdTe

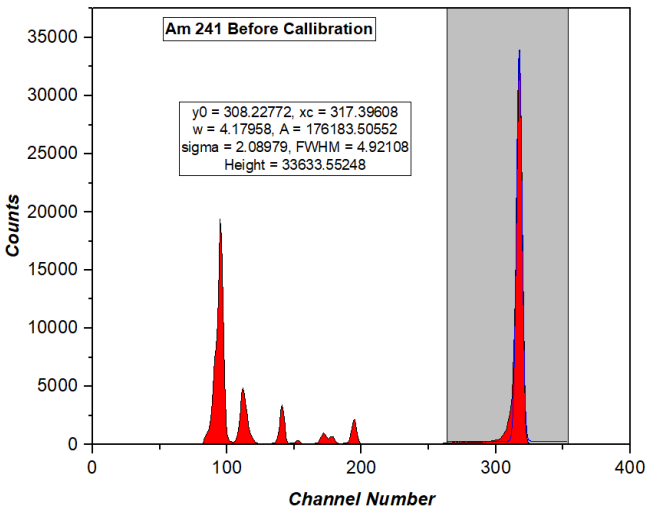

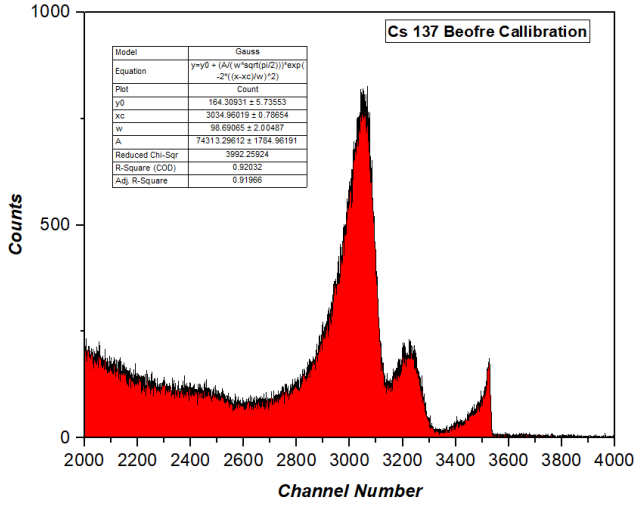

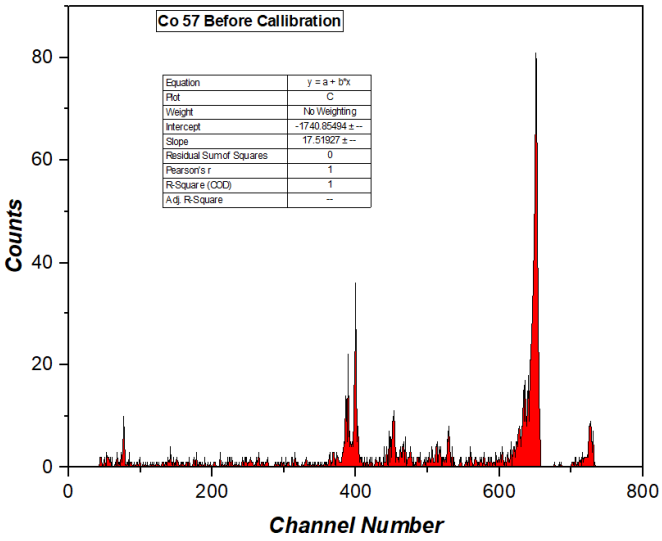

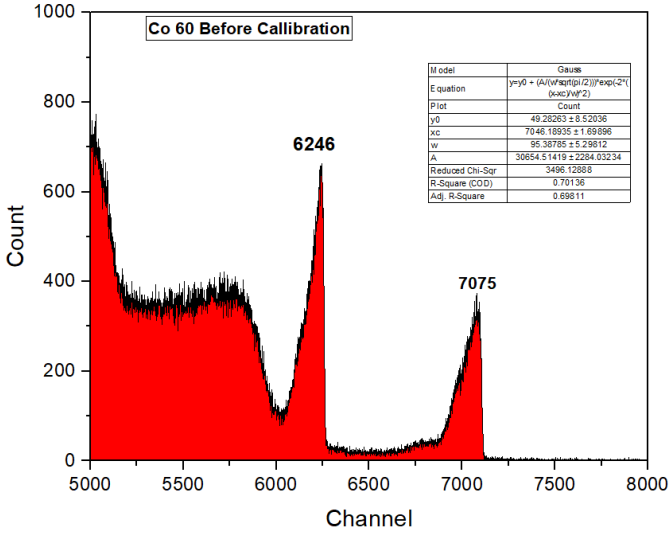

Fig.3 Energy Before Calibration by using four types of isotopes Am-241, Co-60 and Co-57 and Cs-137 by CdTe

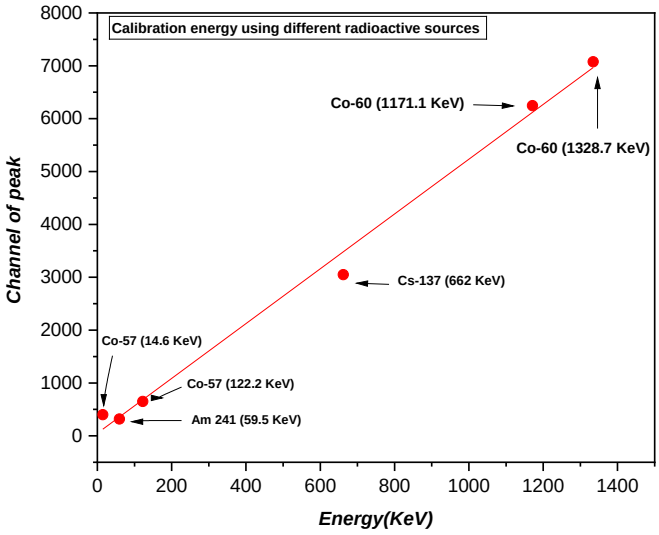

Fig.4 Energy calibration function

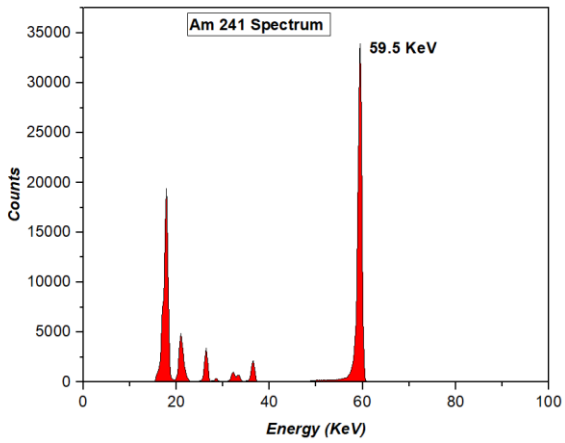

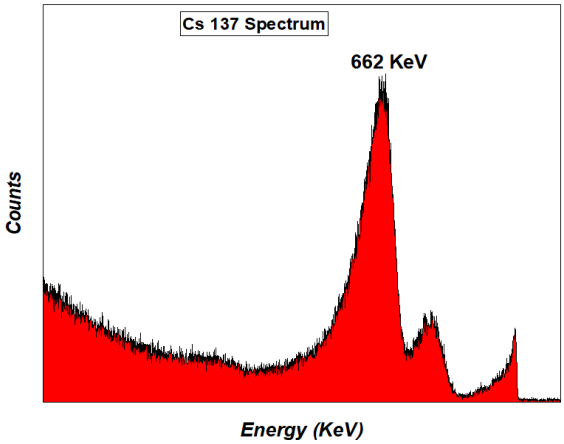

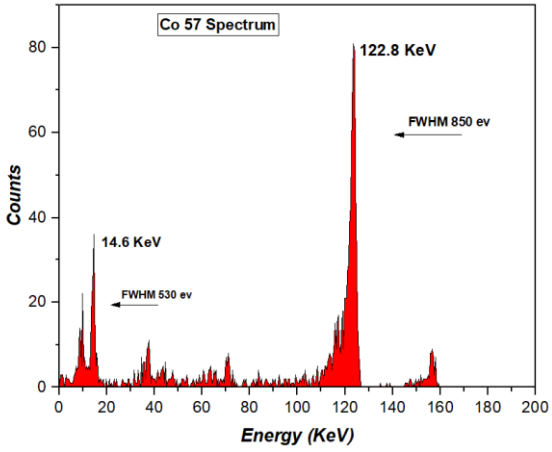

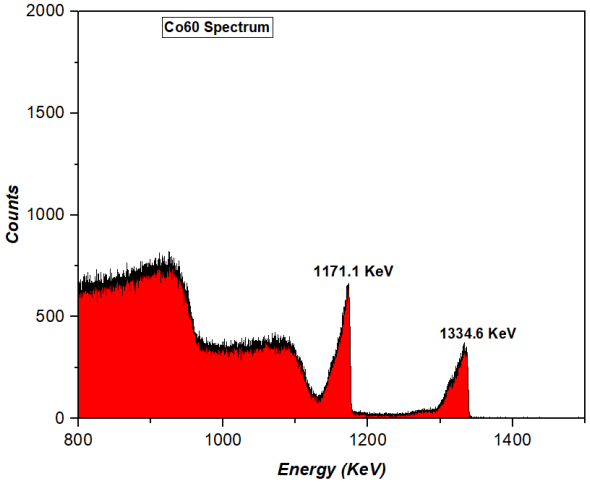

Fig.5 Calibration Energy for Am-241, Cs-137, Co-57 and Co-60

2. Scintillator detectors

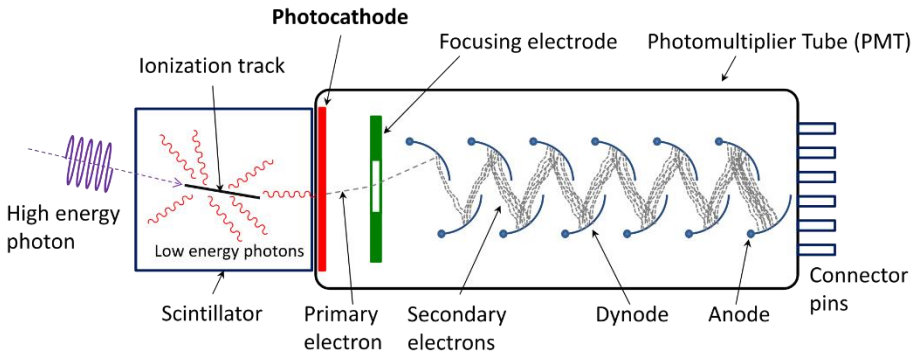

Fig.6 Scheme of scintillator detector

When ionizing radiation is absorbed by the scintillating substance used in these detectors, light is released. An electrical signal is subsequently produced from the light using a photodiode or photomultiplier tube.

• **Organic Scintillators:** Used to detect beta particles, these devices are made from organic materials like plastics or liquids.

• **Inorganic scintillators:** These are effective at detecting gamma rays and are frequently fabricated from crystals like sodium iodide (NaI).

LaBr Scintillator Detector

A lanthanum bromide crystal is used as the scintillating material in the $LaBr_3$ (Lanthanum Bromide) detector, a form of scintillation detector. These detectors are very useful for gamma-ray spectroscopy because of their quick response times and outstanding energy resolution. When compared to conventional scintillators such as sodium iodide (NaI), these detectors offer noticeably superior energy resolution. This high resolution allows for more precise identification and measurement of gamma-ray energies. Besides, the scintillation light decay time in $LaBr_3$ crystals is very short, typically around 16 ns. This fast response enables high count rate capability and reduces the chances of pulse pile-up. $LaBr_3$ crystals produce a high light yield, which results in strong signals that improve the signal-to-noise ratio and enhance the detector's overall performance. It has an intrinsic resolution of about 2.5% at 662 keV (from a Cs-137 source), which is much better than the 6-7% resolution of NaI (Tl) detectors. The better resolution, efficiency and relatively short decay time (16 ns) allow these detectors to be

used with more complex spectra than scintillation detectors as well as in other applications previously thought to be too demanding for any scintillation detector.

Calculation of resolution of $LaBr_3$ at different applied voltages

The LaBr3 detectors' relatively strong intrinsic background from the decay of 138La makes them unsuitable for low-level applications. The resolution of LaBr detectors refers to their capacity to identify the energy of incoming radiation and distinguish it from neighboring energy peaks. It is computed by dividing the peak's full width half maximum (FWHM) by the centroid's location. Where,

$$\boldsymbol{Resolution} = [\frac{\boldsymbol{\sigma}}{\boldsymbol{Mean}} \times \boldsymbol{2.35}]\, \boldsymbol{x}\, \boldsymbol{100}$$

The energy resolution of the detector is a measure of its ability to discriminate between closely spaced energy peaks. The ability to distinguish between neighboring energy peaks is strengthened by a reduced energy resolution, allowing for the identification of individual radionuclides or decay processes in the radiation spectrum.

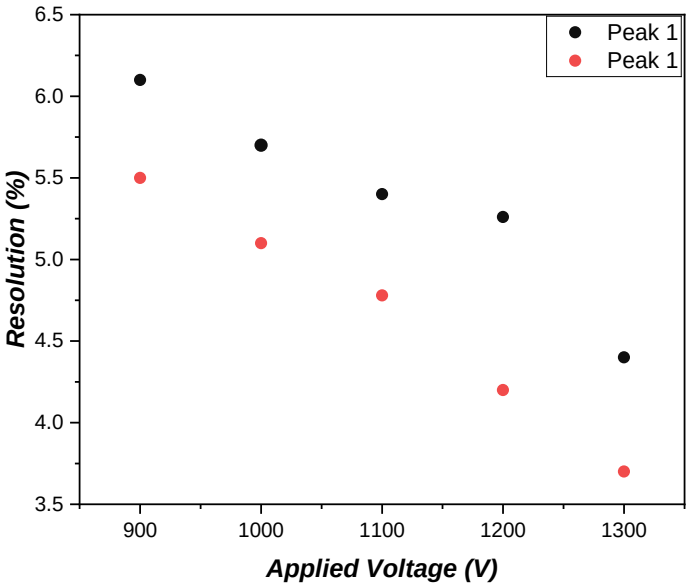

Fig.7 The relation between resolution and applied voltage for $LaBr_3$ detector.

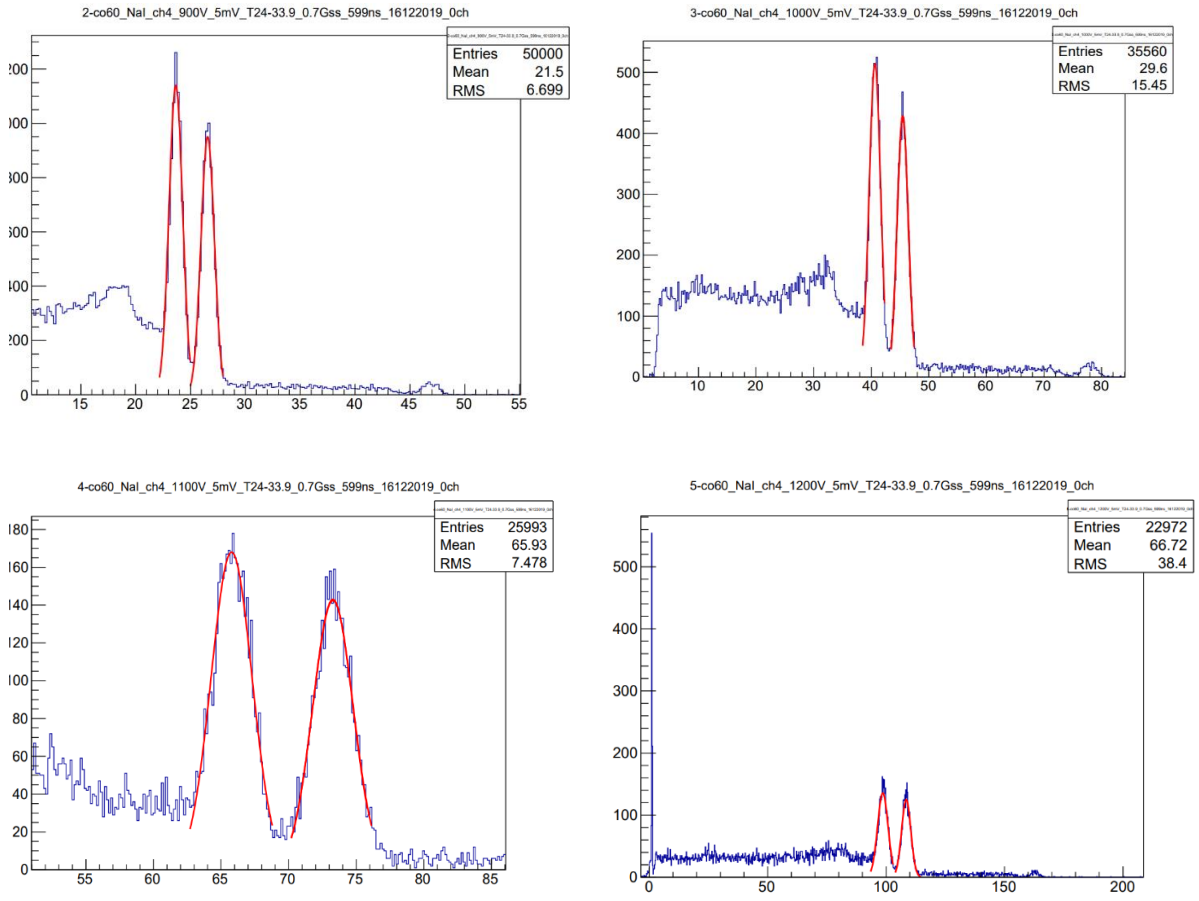

Fig.8 spectrum of Co-60 using $LaBr_3$ detector at 900,1000,1100,1200 applied voltages

For applications requiring high-resolution detection of Co-60 emissions, the resolution of a $LaBr_3$ detector for detecting gamma emissions improves and increases significantly with increasing applied voltage. This improvement in resolution is attributed to the greater signal-to-noise ratio at higher voltages, which allows for more precise discrimination of the gamma-ray energies. Therefore, optimizing the applied voltage in $LaBr_3$ detectors is crucial for achieving superior performance in gamma spectroscopy. This finding emphasizes the significance of carefully tuning detector operating conditions to improve the accuracy and dependability of radiation measurements in both research and practical applications.

Calibration energy using $LaBr_3$ detector

Illustrating the relationship between the energy associated with a particular channel's number (mean). Consequently, a source of known energy peaks (in this case, Co-60 and Cs-137) will be employed to obtain the relation. The initial peak on the spectrum is not an energy peak from either element; rather, it is noise that resulted from the detector's resolution. The energy peak of cesium-137 is the first one from the left. Cobalt-60, however, has three peaks. By utilizing the ROOT software to create a Gaussian fit, the channel number (mean) is found. A calibration curve and the line equation are produced from the plot of energy vs. channel number (mean).

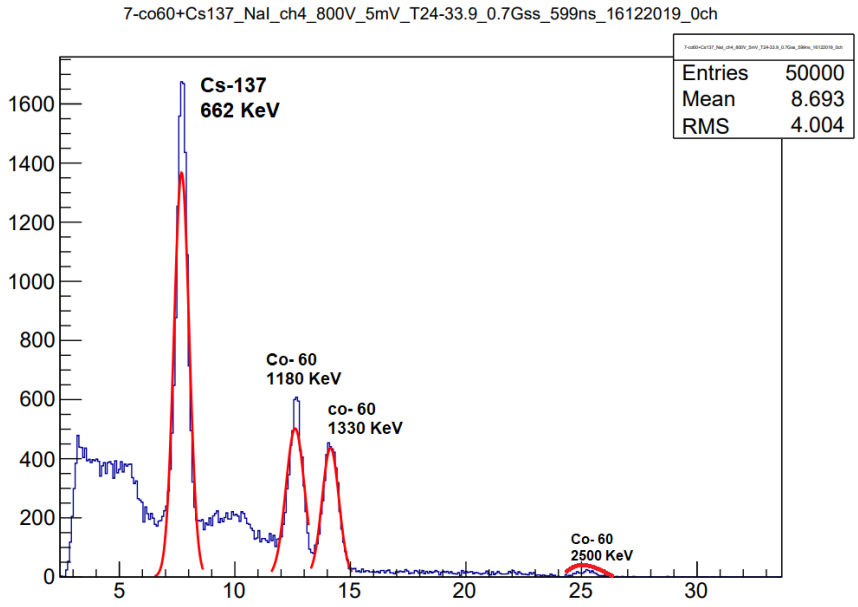

Fig. 9, The energy spectrum of Cs-137 and Co-60 from $LaBr_3$ detector measurements at 800V.

Element	Energy (KeV)	Channel Number (Mean)
Cs-137	662	7.69
Co-60	1180	12.61
	1330	14.14
	2500	24.61

Table (1) Mean and energy of Cs-137 and Co-60 peaks from $LaBr_3$ detector

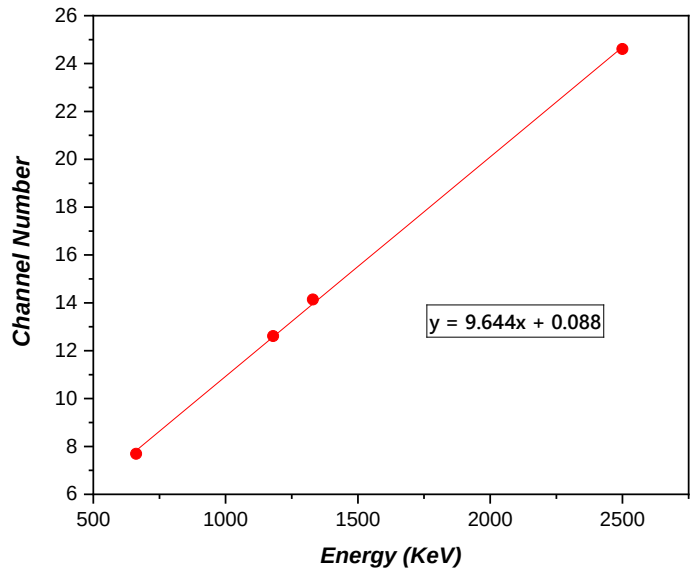

Fig. 10 Energy calibration function for Cs-137 and Co-60 spectrum from $LaBr_3$ detector measurements.

Bismuth Germinate (BGO) Detector

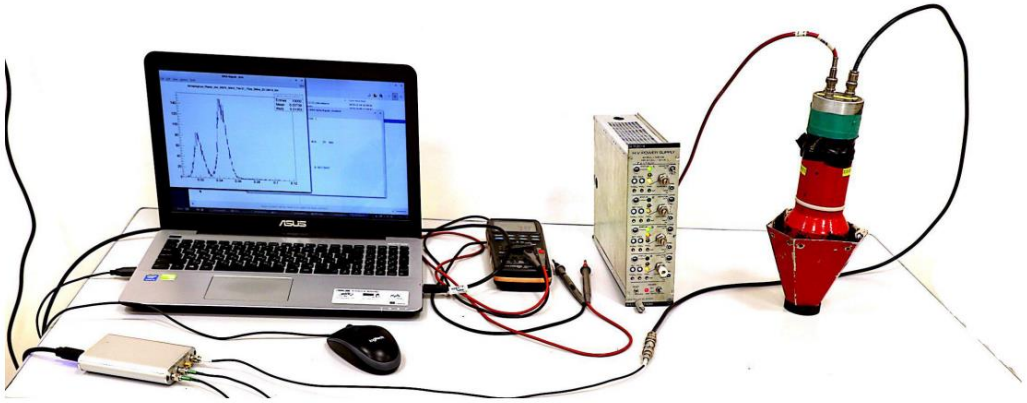

Fig. 11 BGO detector

BGO detector is a kind of scintillation detector that uses Bi4Ge3O12, a high-density and high Z (atomic number) scintillation material. This material is perfect for detecting high-energy radiation such as X-rays and gamma rays since it is very effective at absorbing gamma rays. In addition, it is non-hygroscopic and mechanically strong. Because of its large effective atomic number (Z), BGO increases the possibility that Reducing inter-crystal scatter and enhancing detection efficiency, BGO detectors are employed in positron emission tomography (PET) detectors, radiation detection, medical imaging, radiopharmaceuticals, security surveillance, and geographic

surveying, among other fields. Resolution Fitting graphs for various applied voltages and obtaining the Main and Sigma of peaks, one can then evaluate Resolution using the following equation:

$$\boldsymbol{Resolution} = \left[\frac{\boldsymbol{\sigma}}{\boldsymbol{Mean}} \times \mathbf{2.35}\right] \boldsymbol{x}\ \mathbf{100}$$

Applied Voltage	Mean	Sigma	Resolution %
1200	1.39	0.618	104.4
1300	1.37	0.268	44.59
1400	1.92	0.291	35.49
1500	2.98	0.459	35.48
1600	4.40	0.576	30.76
1700	6.10	0.774	29.81
1900	10.6	1.292	28.6
2000	13.60	1.562	26.95

Table (2) Resolution (%) of BGO detector corresponding to the applied voltage

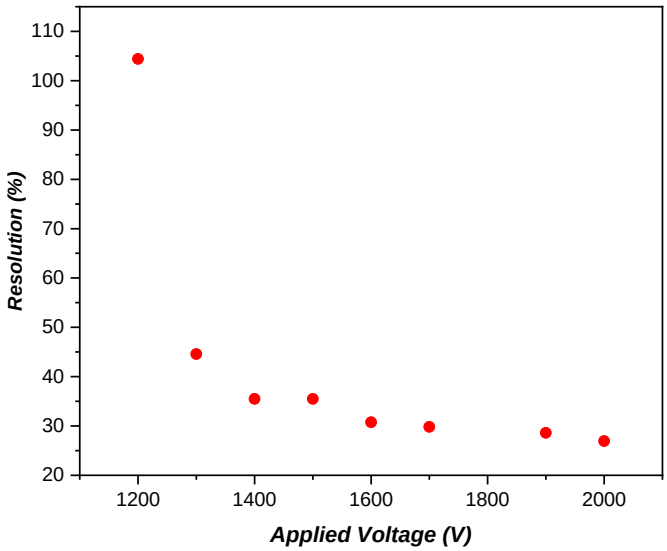

Fig. 12 The relation between resolution and applied voltage for BGO detector

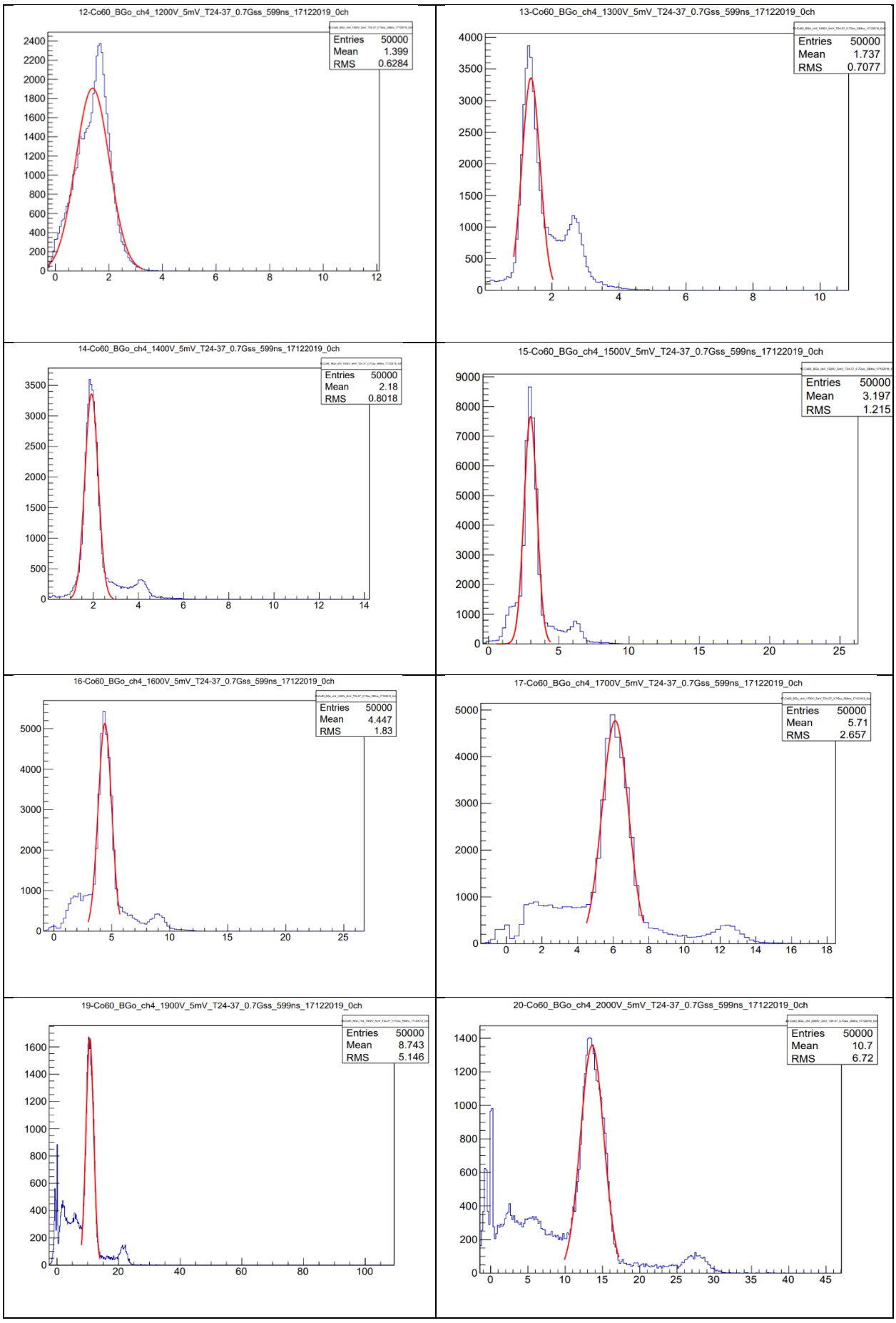

Fig. 13 spectrum of Co-60 using BGO detector at applied voltages from range 1200 to 2000V.

Calibration energy using BGO detector

A link between the number of a certain channel (mean) and its associated energy is produced via calibration. Thus, a source of known energy peaks (in this example, cobalt and cesium) will be employed to obtain the relation. There is no energy peak from either element at the first peak on the spectrum; rather, it is noise caused by the detector's resolution. The energy peak of cesium-137 is the first one from the left. In contrast, Cobalt-60 exhibits two peaks. Using the ROOT program, a Gaussian fit is made to get the channel number (mean). The line equation is produced by creating a calibration curve using the plot of energy vs. channel number (mean).

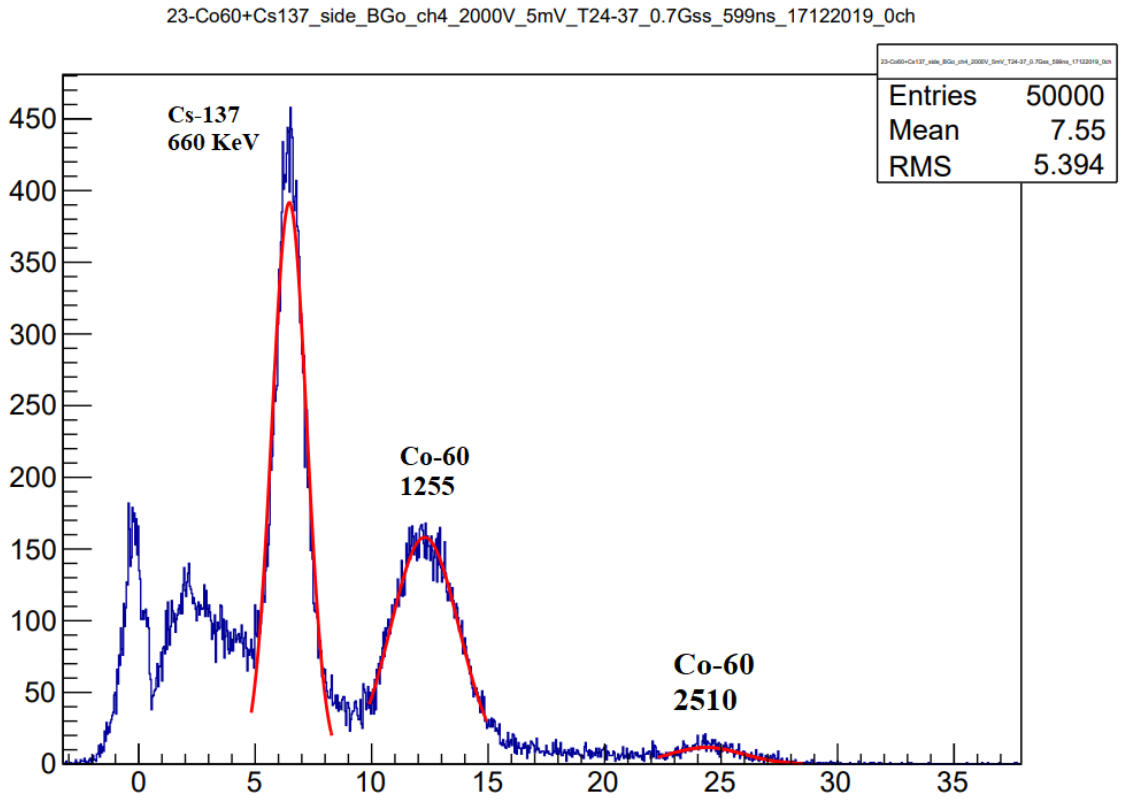

Fig. 14 The energy spectrum of Cs-137 and Co-60 from BGO detector measurements at 2000V. **Calibration equation is**

$$y = 9.7284x + 0.0458$$

Element	Energy (KeV)	Channel Number
Cs-137	660	6.47
Co-60	1255	12.27
Co-60	2510	24.57

Table (3) Mean and energy of Cs-137 and Co-60 peaks from a BGO detector.

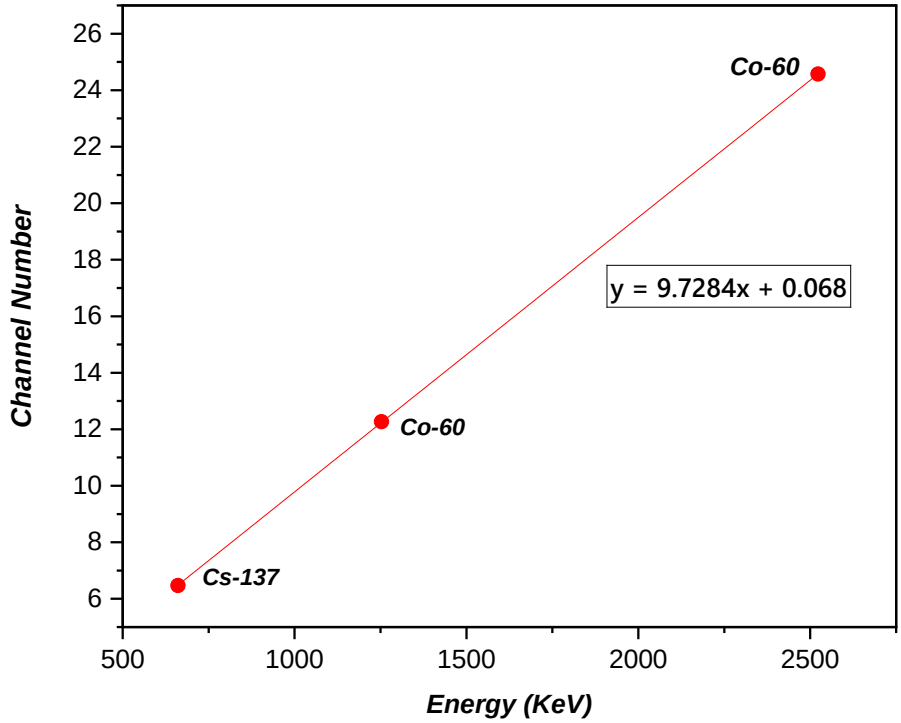

Fig.15 Energy calibration function for Cs-137 and Co-60 spectrum from BGO detector measurements.

Identification of Unknown Sources

Fitting five unknown peaks and get the Mean, then substitute in calibration function to get the Energy of unknown element and finally compare between energies.

$$y = 1.45953 + 9.50263x$$
$$y = 4.488$$
$$4.688 = 1.45953 + 9.50263x$$
$$x = 0.34$$

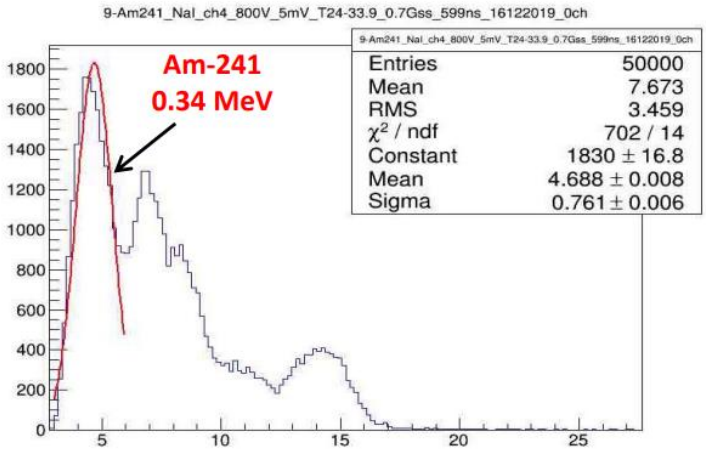

Fig.16 energy calibration using BGO identification of Unknown Source

Application of Monochromator in Determining Graphite Atomic Spacing

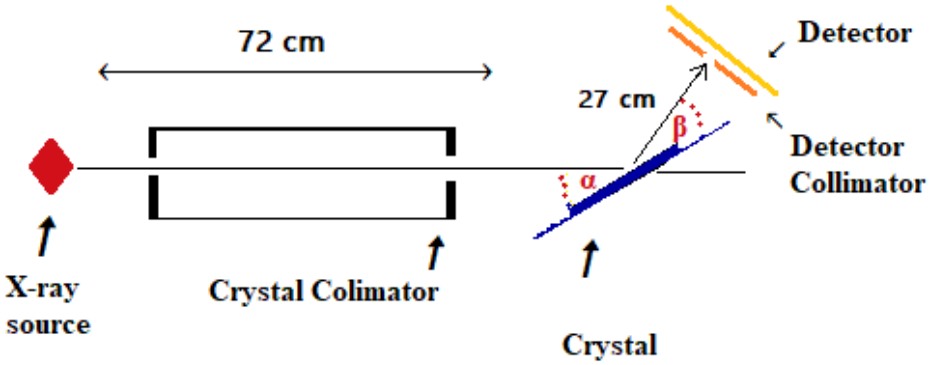

Fig.17 illustrate conceptional design of monochromator

A monochromator is an essential optical device used in various scientific and industrial applications to isolate and select specific wavelengths of light from a broader spectrum. Its advantages are numerous and particularly valuable in fields like spectroscopy, photonics, and medical imaging. The monochromator works by first collimating the broad-spectrum light, then dispersing it into its component wavelengths using a diffraction grating or prism. The focusing lens or mirror directs the dispersed light onto the exit slit, which isolates the desired wavelength. The isolated wavelength can then be detected or used in various applications, such as spectroscopy. Precise measurements of X-ray wavelengths and their interactions with the material are necessary to compute the spacing distance between graphite atoms using a monochromator. For several reasons, this procedure is essential to materials science and crystallography.

Knowing a material's atomic structure is essential for protecting against and detecting nuclear radiation. The accurate measurement of interatomic spacings in a material, like graphite, helps in radiation detector calibration and performance improvement. This section describes how the spacing between graphite atoms at different energies was investigated using a monochromator-assisted X-ray diffraction (XRD) technique.

Advantages of Using a Monochromator

• **High Resolution:** Generates diffraction data with a high degree of resolution, enabling more precise structural calculations.
• **Decreased Background Noise:** In diffraction patterns, monochromatic X-rays increase the signal-to-noise ratio by reducing background noise.
• **Consistency:** Makes sure measurements are repeatable and consistent, which is necessary for accurate data.

Bragg's Law and X-Ray Diffraction

- The spacing distance between graphite atoms can be determined using Bragg's Law, which relates the wavelength of incident X-rays to the diffraction angles and the distance between atomic planes in a crystal. Bragg's Law is given by:

$$d = n \lambda / 2 \sin(\alpha)$$

where n is the number of peaks, λ is the wavelength of the X-rays, d is the interplanar spacing, and α is the crystal angle. The detector angle is twice the crystal angle Where,

$$\beta = 2\alpha$$

A monochromator was used with an X-ray diffraction apparatus to obtain precise measurements of the interatomic spacings in graphite. The purpose of the monochromator was to separate X-ray wavelengths from a wide spectrum produced by an X-ray source. We ensured exceptional precision in the resulting diffraction patterns by choosing monochromatic X-rays.

Utilizing a monochromator and a high-intensity X-ray source, X-rays were produced. To filter and choose the optimal X-ray wavelength, a monochromator—typically a crystal monochromator made of silicon (Si) or germanium (Ge)—was utilized. The graphite sample was exposed to monochromatic X-rays, and the diffraction patterns were noted. Diffraction and Data Gathering: By calculating the angles at which the graphite's atomic planes scattered X-rays, diffraction patterns were discovered. The

monochromator made it possible to precisely adjust the incident X-ray wavelength, which made it possible to analyze in-depth how various energy levels impacted the diffraction patterns.

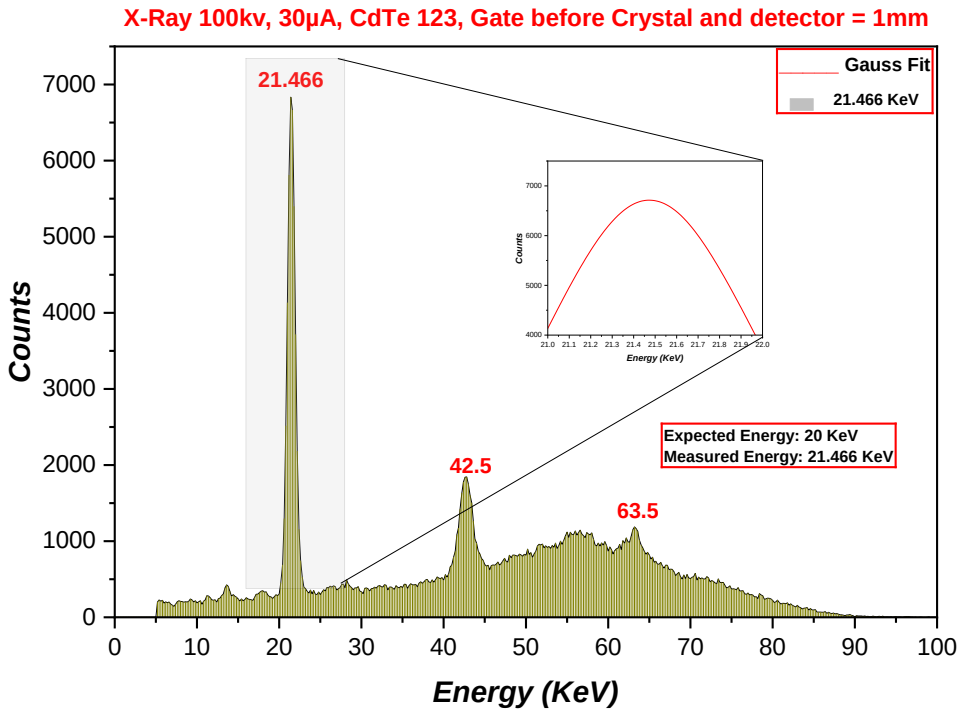

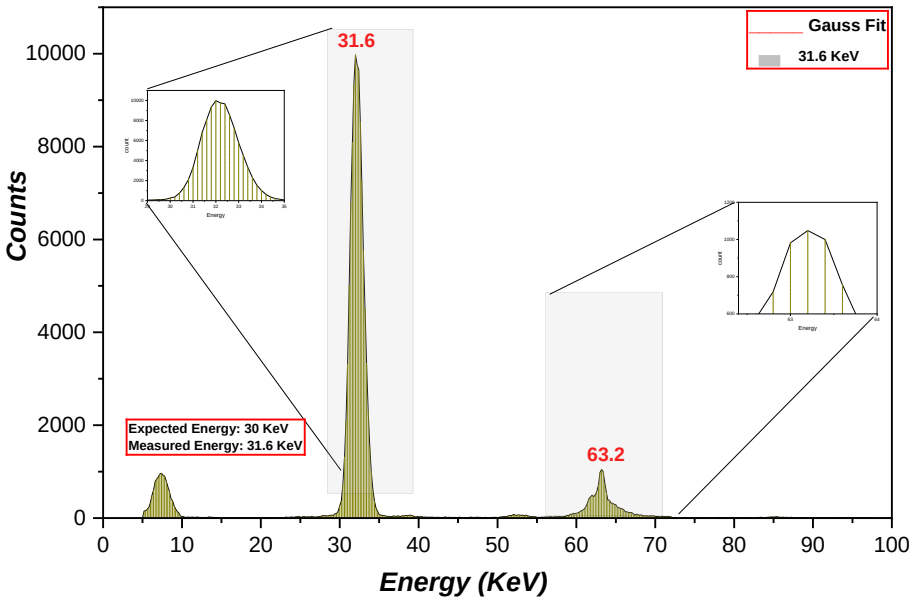

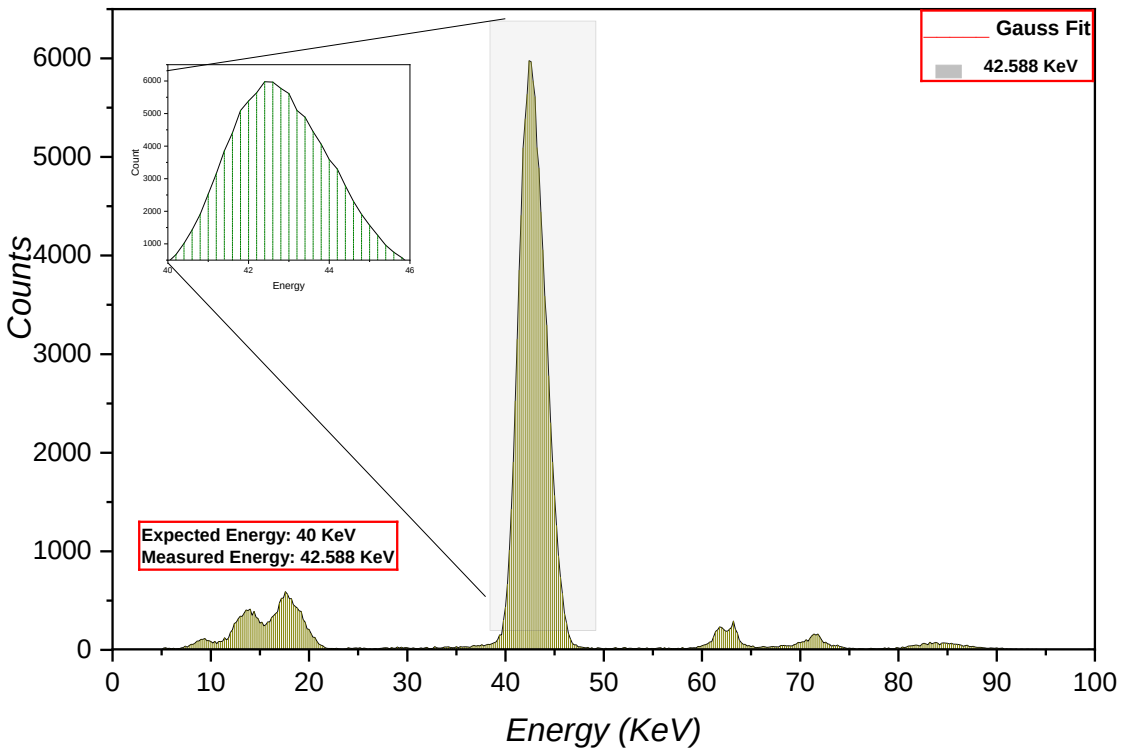
Gauss Fit
42.588 KeV
Expected Energy: 40 KeV
Measured Energy: 42.588 KeV
Counts
Energy (KeV)
Count
Energy

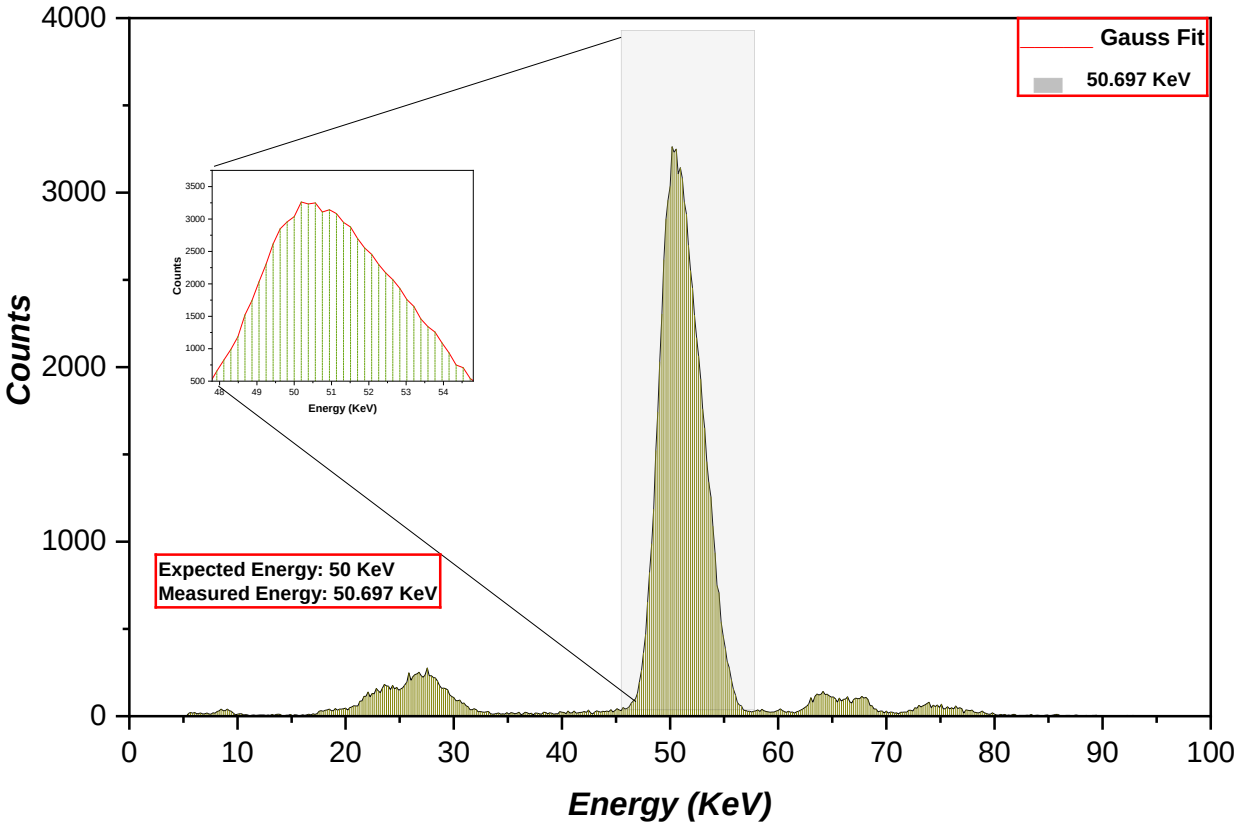
Gauss Fit
50.697 KeV
Expected Energy: 50 KeV
Measured Energy: 50.697 KeV
Counts
Energy (KeV)

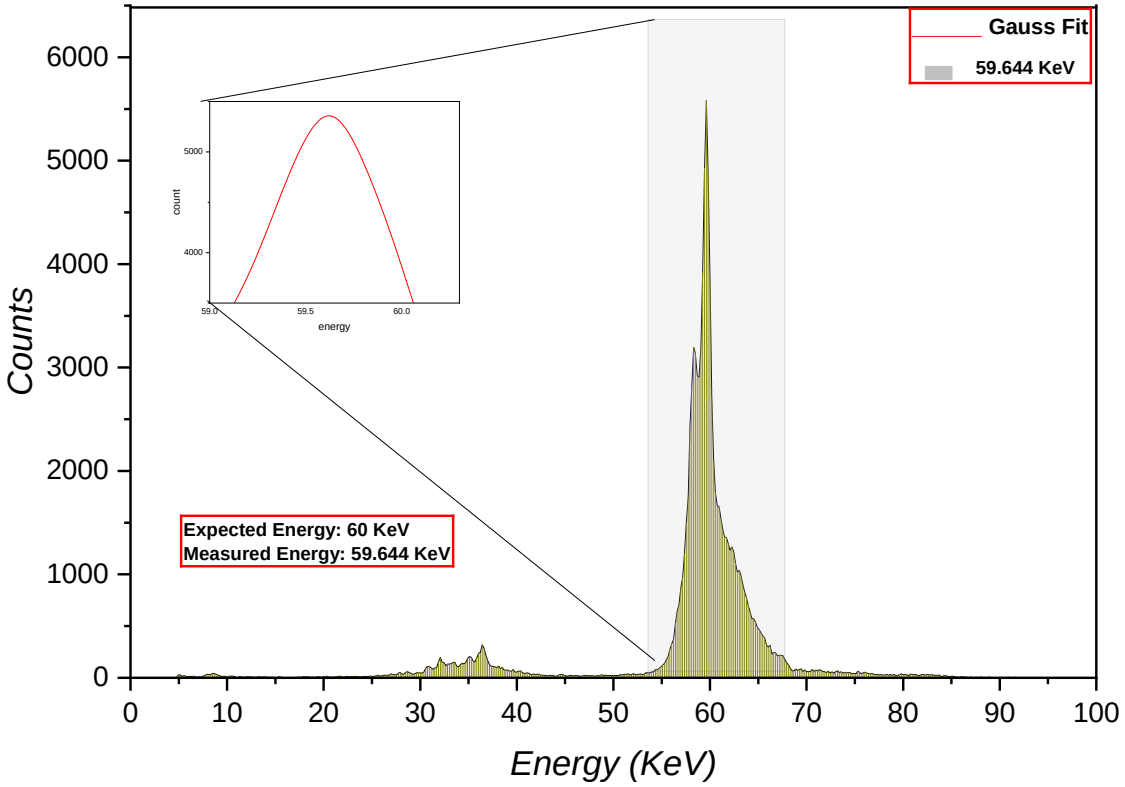
Gauss Fit
59.644 KeV
Expected Energy: 60 KeV
Measured Energy: 59.644 KeV
Counts
Energy (KeV)
count
energy

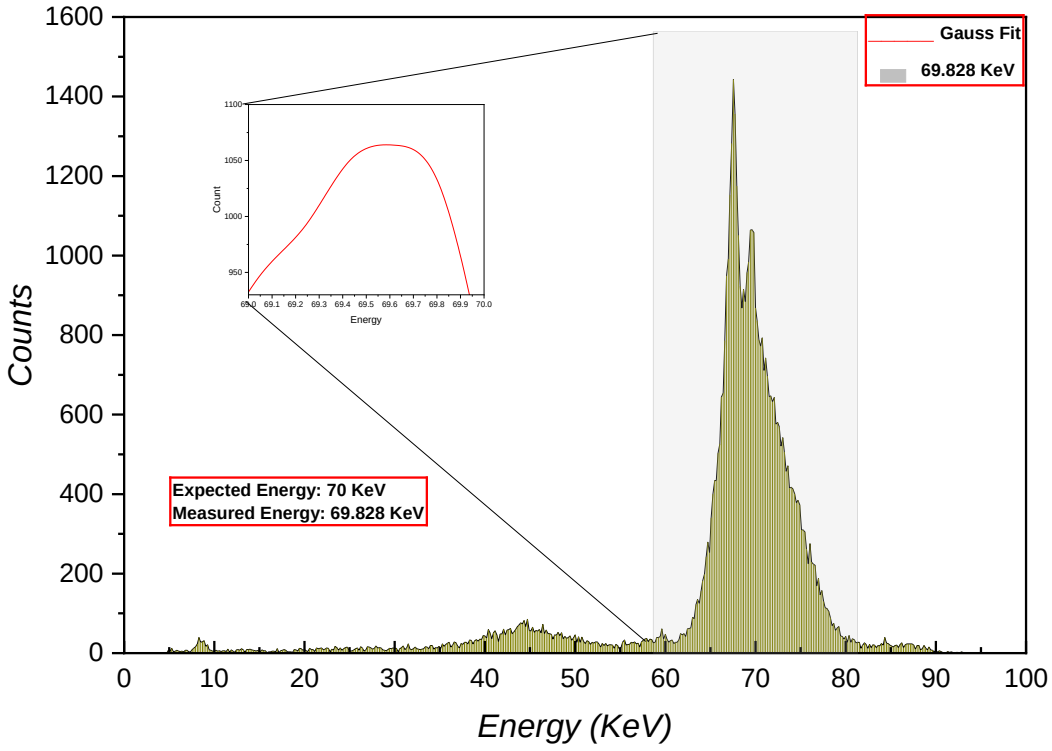
Gauss Fit
69.828 KeV
Expected Energy: 70 KeV
Measured Energy: 69.828 KeV
Counts
Energy (KeV)
Count
Energy

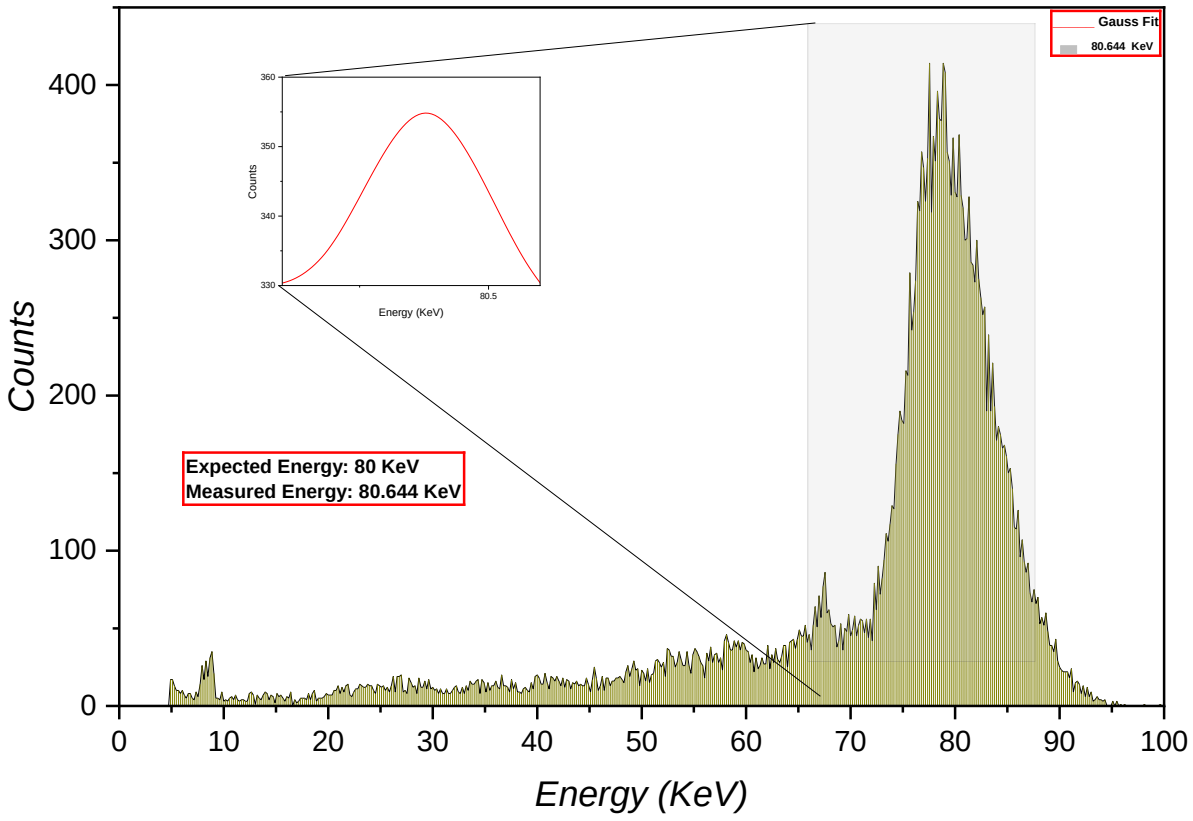

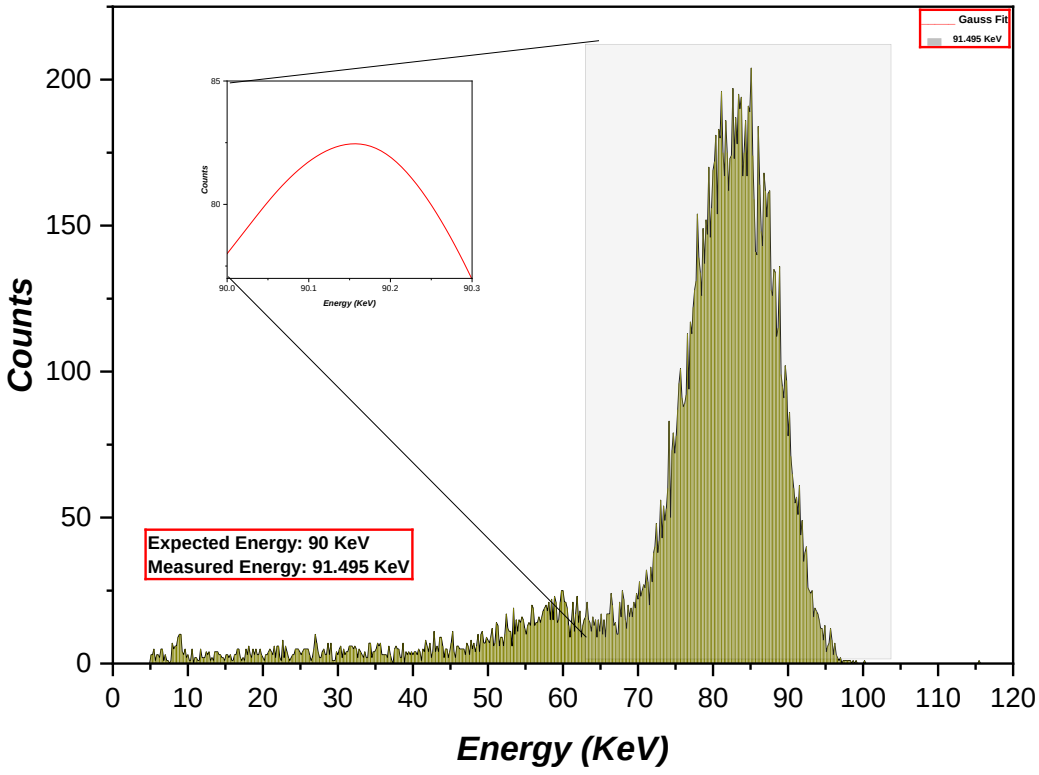

Fig.18 the relation between the energy and counts at different energy levels from ranges 20V to 90V

Crystal Angle	Expected Energy	Measured Energy	K
5.2	20	21.6	1.08
3.49	30	31.6	1.05
2.62	40	42.5	1.06
2.09	50	50.7	1.014
1.74	60	59.6	0.99
1.49	70	69.7	0.99
1.30	80	80.5	1.006
1.164	90	90.5	1.006

Table (4) measured and expected energies at different crystal angles

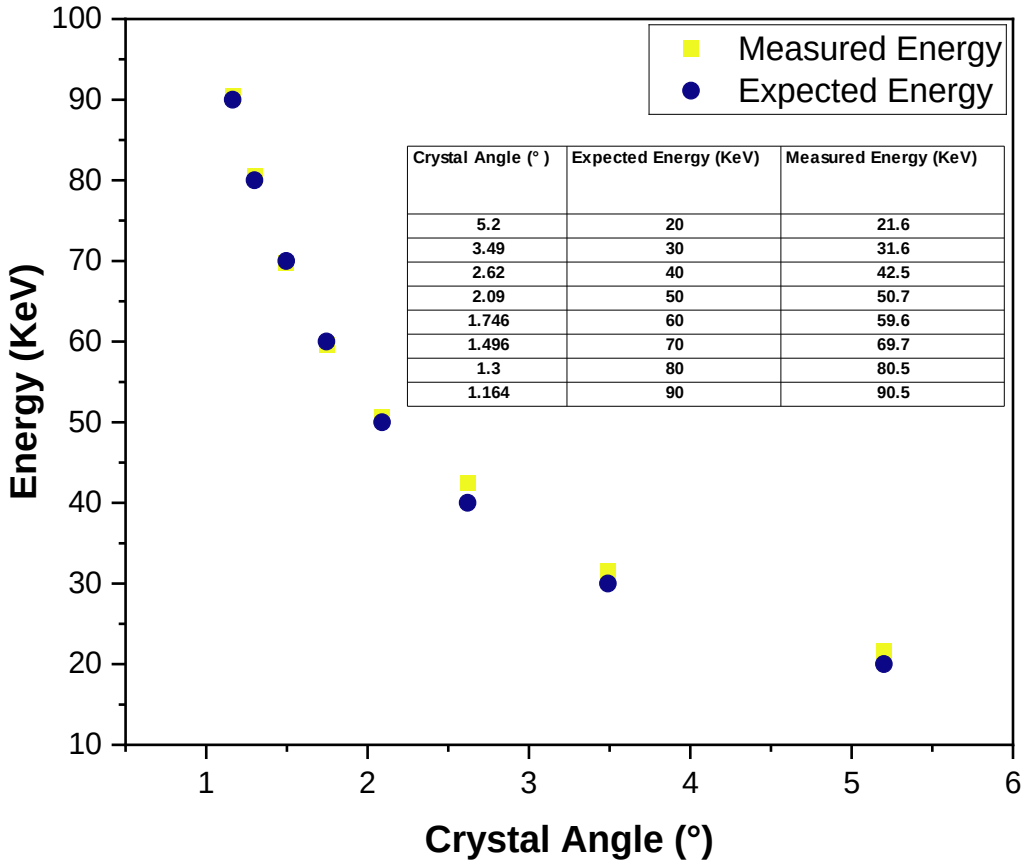

Fig. 19 relation between crystal angle and both measured and expected Energy

Discussion

High-resolution information on the atomic spacing in graphite was obtained using X-ray diffraction using a monochromator. The precision with which X-ray wavelengths were chosen reduced errors and enhanced measurement accuracy. The material's response to varying radiation energies was highlighted by the results, which displayed fluctuations in the interplanar spacings with changes in the energy levels of the incident X-rays. This comprehensive knowledge of the atomic structure of graphite is essential for radiation detector calibration. Radiation protection systems are made safer and more effective when detectors are calibrated accurately, which guarantees that they can monitor radiation doses with reliability. The knowledge gathered from this research also benefits the larger field of material science, since accurate atomic measurements are necessary to create innovative materials with certain characteristics.

Angle α	E (peaks) ,KeV	E	Λ ,nm	d ,nm
5.2	21.466 42.5 63.5	21.6	0.057	0.942
3.49	31.6 63.2	31.6	0.039	0.641
2.62	42.5	42.5	0.029	0.317
2.09	50.7	50.7	0.024	0.328
1.74	59.6	59.6	0.020	0.328
1.49	69.7	69.7	0.017	0.326
1.30	80.5	80.5	0.015	0.330
1.16	90.5	90.5	0.0137	0.320

Table (5) Calculation of spacing distance and wavelengths at different energy levels.

The wavelength of incident radiation decreases with increasing energy, and this allows for a more precise measurement of the spacing d between atomic planes in a crystal lattice since shorter wavelengths may probe smaller distances. This relationship underpins a multitude of scientific and technological applications in domains like materials science, chemistry, and structural biology. It is essential to characterize materials by diffraction techniques. The precision, dependability, and safety of radiation therapy treatments for cancer patients are improved using graphite diffraction in detector calibration and dosimetry. It makes use of basic physics and materials science concepts to enhance clinical results and promote continuous improvements in medical

radiation technology. In conclusion, using a monochromator to calculate the spacing distance of graphite atoms is essential for obtaining precise and accurate measurements in X-ray diffraction experiments. the experimental measurement of graphite spacing distance using a monochromator supports a variety of scientific and technological applications in physics, materials science, and other fields by providing important information about the crystal structure of graphite.

Pixel Detector

A pixel detector consists of two chips. The first chip/sensor chip is a semiconductor diode with one pixelated contact and one common backside coated by thin layer of nickel, while the second chip is composed of read-out electronics for every pixel. Bump-bonding technique is used to connect both chips. Pixel sizes range from 100 to 400 µm.

Composition parts of PD
1. Sensor chip
2. solder pumps
3. read-out electronics chip

- **The size of the sensor:** 1.5x1.5 cm
- 256 x 256 pixels (65.536 pixel)
- **Pixel size:** 55µm x 55µm.
- **Si Thickness:** 300 µm

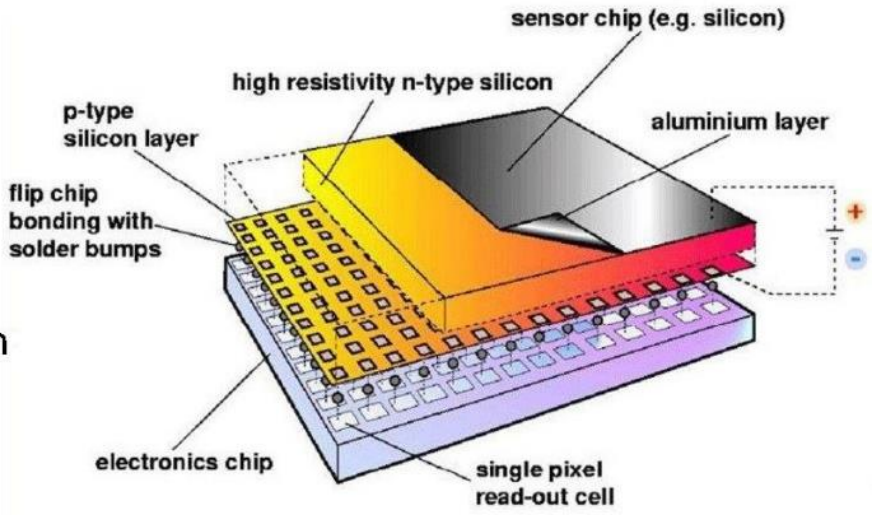

Fig. 20 Pixel detector

Determination alpha particles range with (Am-241) in Air at energy 4 MeV Using pixel detector

Positively charged particles known as alpha particles are released spontaneously from the nuclei of some radioactive materials. With an electrostatic charge of +2, it is a helium ion. The components of alpha particles are two protons and two neutrons bonded together.

Range is the distance that alpha particles travel before losing all their kinetic energy and recombining with electrons to produce stable helium atoms.

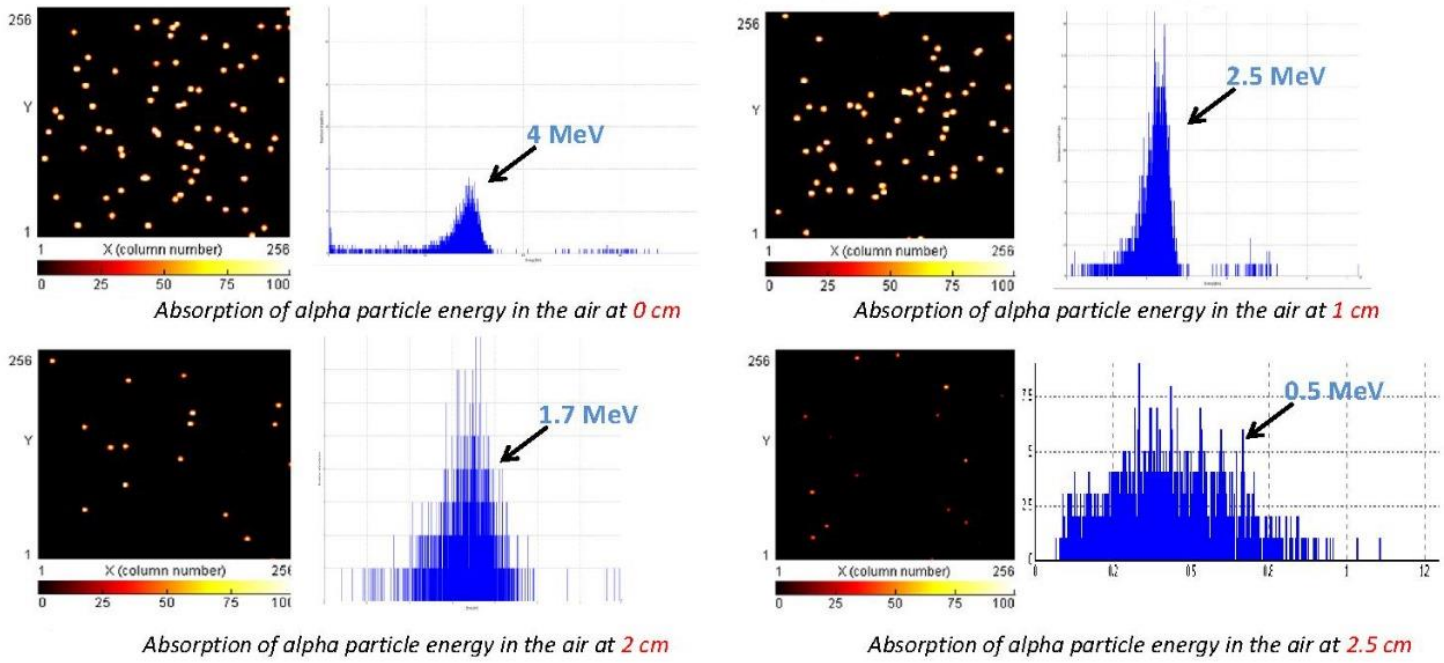

Fig. 21 Absorption of alpha particle energy in air at different thicknesses

Determination of alpha range in air using SRIM (Monte Carlo simulation)

SRIM is a software that enables users to simulate and analyze various phenomena such as ion penetration, energy deposition, and particle range within solid materials. Because alpha particles are thousands of times heavier than atomic electrons, which cause them to gradually lose energy, alpha particles travel in nearly straight paths. In this experiment, we will use a pixel detector to measure the alpha particle's range in the air by varying the distance between the detector and the alpha source until no alpha particle is detected. From this distance, we obtain our maximum range, which is approximately 3 c.

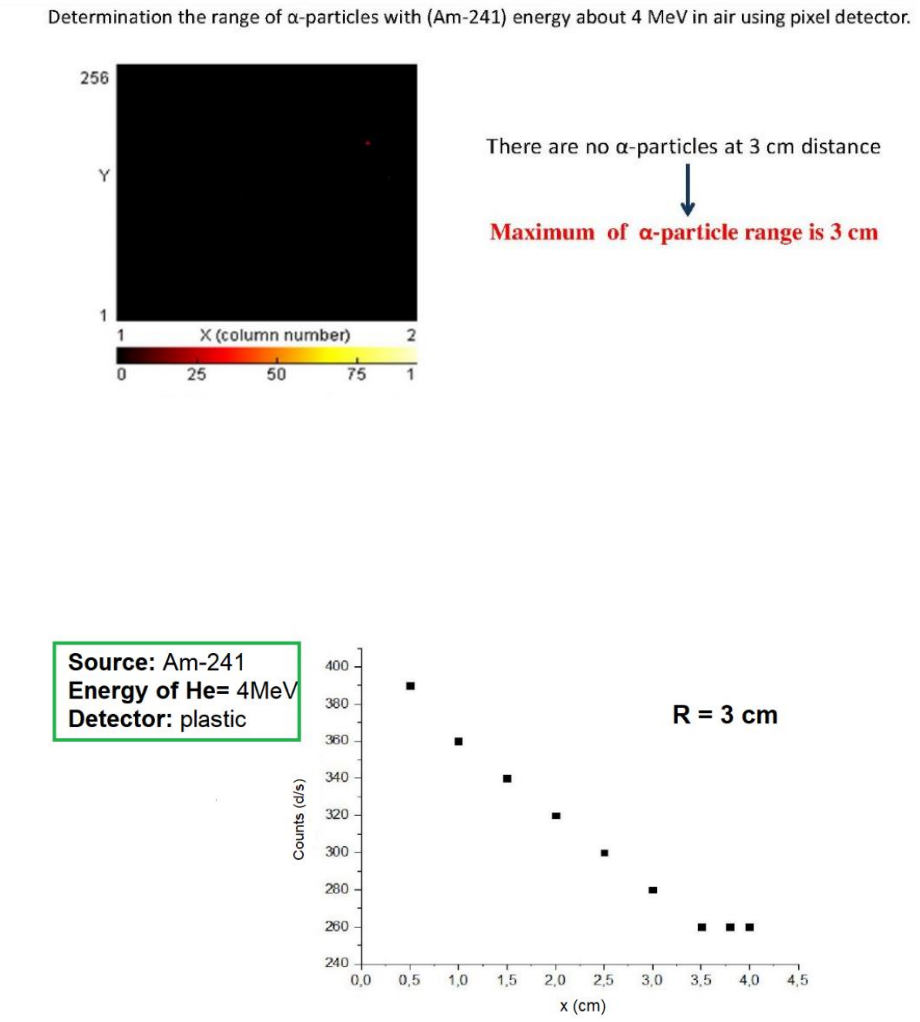

Fig. 22 Maximum of alpha particles range

It can be challenging to determine this range practically, thus SRIM software can perform a Monte-Carlo simulation of the incidence of an alpha particle on various materials, including air, as seen in the following picture.

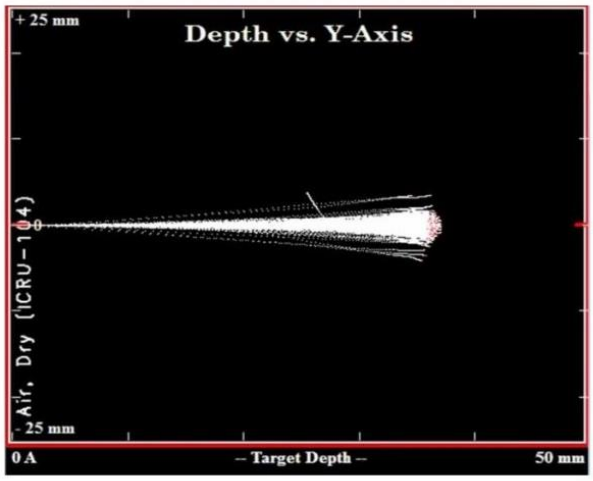

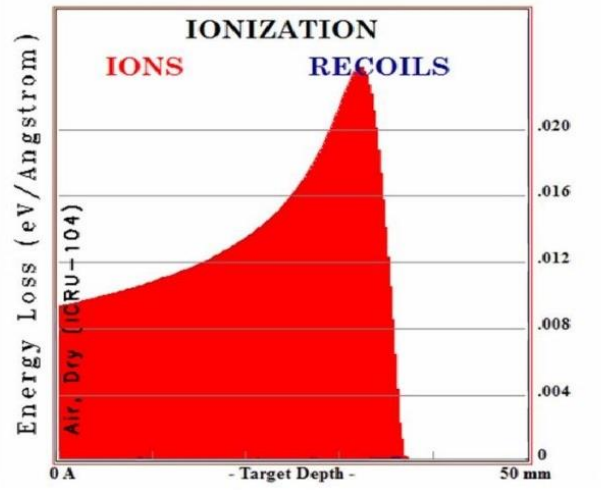

Fig. 23 Depth for alpha radiation in air

Fig. 24 Ionization – Depth graph for alpha radiation

A software program called Stopping and Range of Ions in Matter (SRIM) is used to determine the stopping and range of ions as they move through different kinds of materials. It is extensively employed in the domains of ion implantation, radiation damage, and material science research and is based on the Monte Carlo simulation technique. Important information on ion interactions, such as penetration depth, sputtering rates, and energy deposition, is provided by SRIM. At α = 1500 Kev of energy, this is the outcome.

Attenuation Coefficient

Its known that gamma rays can go through anything which make it import when designing shields as the material of the shield should stop gamma rays before reaching the body so we need to define something named attenuation coefficient which represent the rate of reducing in the number of gamma rays as they pass through material Attenuation coefficient describes the fraction of a beam that is absorbed or scattered per unit thickness of the absorber governed by the following equation:

$$I = \mathrm{I}_0 e\,(-\mu\, x)$$

Where μ is the attenuation coefficient, I is the intensity of radiation at thickness x and Io is the intensity at 0 thickness.

Our research is to determine the attenuation coefficient of (Cu, Al) so that a shield for any radioactive source can be designed, using BGO scintillation detector; 2000V operating voltage; 661 KeV energy from the Cs137 gamma source.

Fig. 25 attenuation coefficient experiment equipment

Determine the attenuation coefficient of radiation in Copper (Cu) and Aluminum (Al) shields

For Al

Thickness(cm)	I/I0
0	1
0.15	0.75573
0.3	0.71623
0.45	0.70569
0.75	0.68596
0.9	0.67155
1.08	0.66103
1.26	0.63939

Table (6) relation between thickness and attenuation for Al

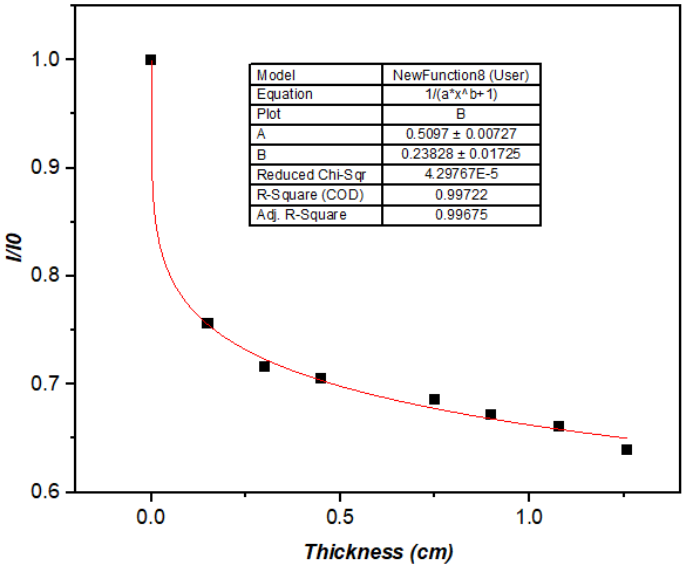

Fig. 26 linear exponential between thickness and attenuation for Al

From the equation y= e $(-0.238x)$ μ = 0.238

For Cubber (Cu)

Thickness(cm)	I/I0
0	1
0.2	0.73931
0.25	0.7357
0.4	0.68065
0.8	0.58611
1	0.53827
1.2	0.48042

Table (7) relation between thickness and attenuation for Cu

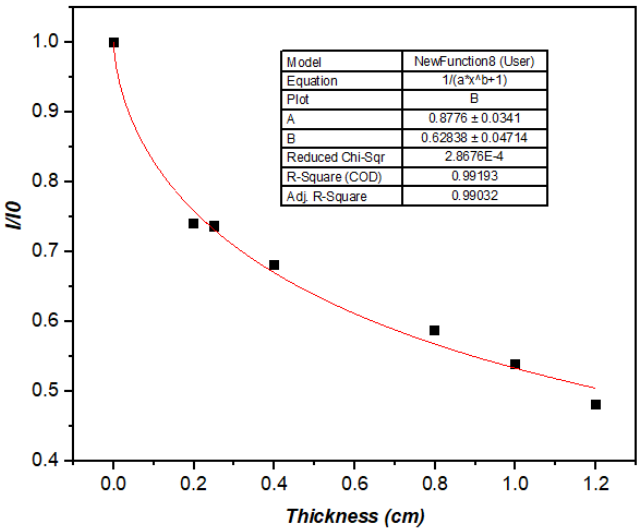

Fig. 27 linear exponential between thickness and attenuation for Al

From the equation y = e $(-0.628x)$ μ = 0.628

A Theoretical Approach in calculating the X-Ray Attenuation Coefficients in Human body Tissues

It is crucial to comprehend how X-rays attenuate as they move through the various bodily tissues to maximize imaging methods and guarantee precise diagnosis. The theoretical calculations used to find the X-ray attenuation coefficients for different tissues, such as tumors, fat, and muscle, are described in detail in this section.

Methodology

Theoretical methods that consider the physical characteristics of the tissues were used to model the attenuation of X-rays in human tissues. The calculations that were done were:

1. Theory of X-Ray Attenuation: The following equation was used to determine the linear attenuation coefficient (μ): $I = I_0 e^{(-\mu x)}$

where μ is the linear attenuation coefficient, x is the tissue thickness, I_0 is the beginning intensity, and the X-ray beam's intensity after passing through the tissue.

2. Tissue Density and Composition: Each type of tissue (muscle, fat, and tumor) was considered in terms of its unique density and composition. The interaction between X-rays and these tissues was modeled using data from databases and current literature.

2. **Energy Dependence** To comprehend how attenuation changes with energy, computations were done for various X-ray energy levels. This is essential for customizing imaging methods to meet various diagnostic requirements.

Results

The theoretical calculations provided the following insights:

1. **Attenuation Coefficients**:

o Because tumors have denser cellular structures than fat and muscle, they have higher attenuation coefficients.
o Fat's reduced attenuation was in line with its increased lipid content and lower density.
o the intermediate values for muscle tissues indicate their distinct density and composition.

2. **Intensity Profiles**

Compared to fat and muscle, the intensity of X-rays was much lower through tumors, emphasizing the significance of energy selection in imaging techniques to improve tumor contrast.

Discussion

The results of the theoretical computations are essential for raising the precision and effectiveness of medical imaging methods. Radiologists can tailor imaging parameters to maximize tumor visualization while avoiding exposure to nearby healthy tissues by knowing the unique attenuation qualities of various tissues.

Conclusion

The theoretical determination of X-ray attenuation coefficients for human tissues provides a foundation for enhancing diagnostic imaging techniques. This approach not only improves the accuracy of detecting tumors but also contributes to the overall effectiveness of radiation protection strategies in medical settings.
Additionally, the measurement of attenuation coefficients of various tissues such as the heart, blood, fats, and tumors help in understanding how radiation interacts with different parts of the body. This knowledge is crucial for optimizing imaging techniques to distinguish tumors from surrounding healthy tissues effectively, thereby enhancing

diagnostic accuracy and treatment efficacy. The use of monochromators to calculate graphite spacing distance at different applied energies further contributes to the precision of radiation measurements. By analyzing the resulting spectrums, researchers can gain valuable insights into the behavior of radiation as it passes through different tissues, leading to better calibration of radiation doses and improved protective measures.

Name		*E (low edge) KeV*	*Integrate %*	*Material + Thickness (cm)*
Filter	**Before**	**12.11**	**100**	**Cu 0.05+ Steel 0.03**
	After	**30.44**	**21.2**	
Air	**Before**	**30.67**	**21.2**	**Cu 0.05+ Steel 0.03+Air 40**
	After	**30.67**	**20.2**	
Fats	**Before**	**30.67**	**20.2**	**Cu 0.05+ Steel 0.03+Air 40+ Fats 10**
	After	**39.12**	**2.77**	
Heart	**Before**	**39.12**	**2.77**	**Cu 0.05+ Steel 0.03+Air 40 + Fats 10+ Heart 10**
	After	**40.28**	**0.37**	
Blood	**Before**	**40.28**	**0.37**	**Cu 0.05+ Steel 0.03+Air 40 + Fats 10+ Heart 10+ blood 10**
	After	**42.61**	**0.049**	
Air	**Before**	**42.61**	**0.049**	**Cu 0.05+ Steel 0.03+Air 40 + Fats 10+ Heart 10+ blood 10 + Air 10**
	After	**42.61**	**0.049**	

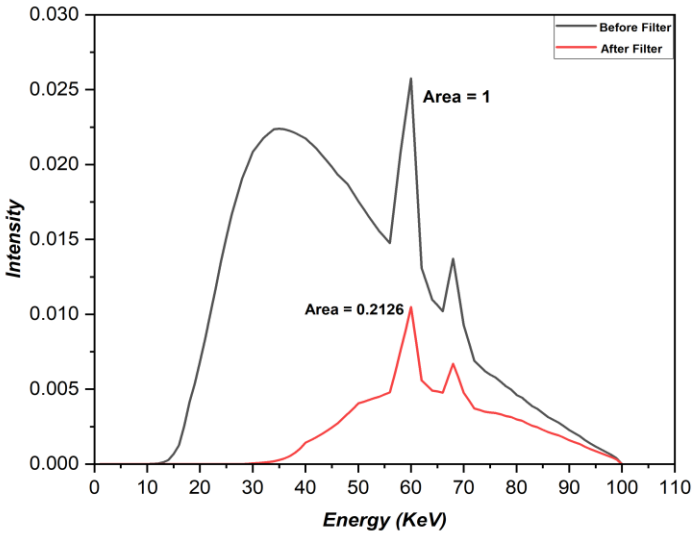

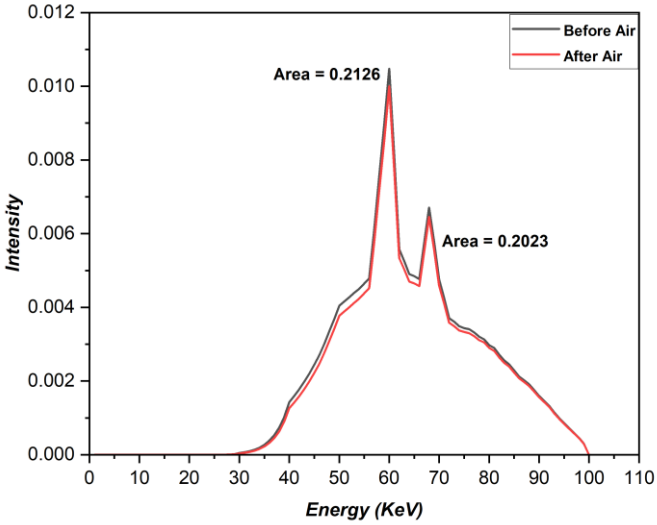

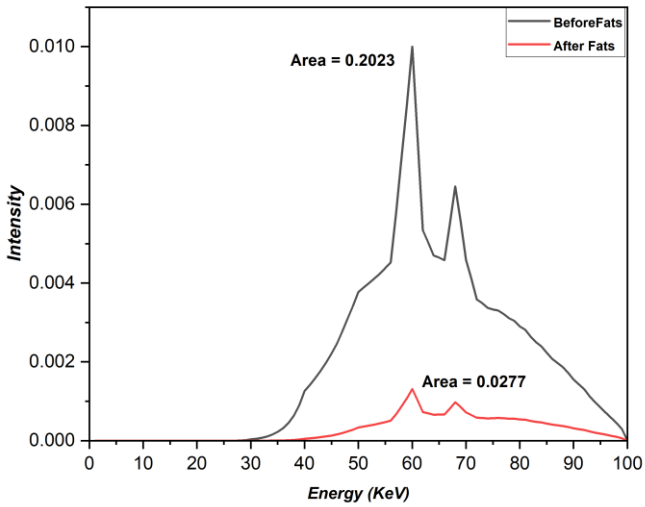

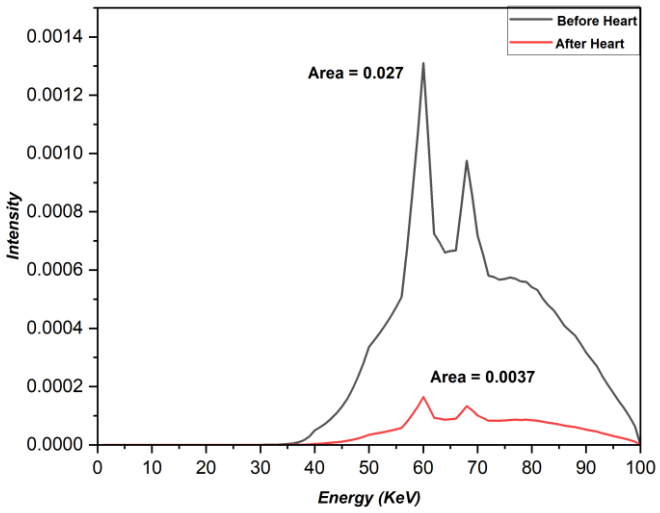

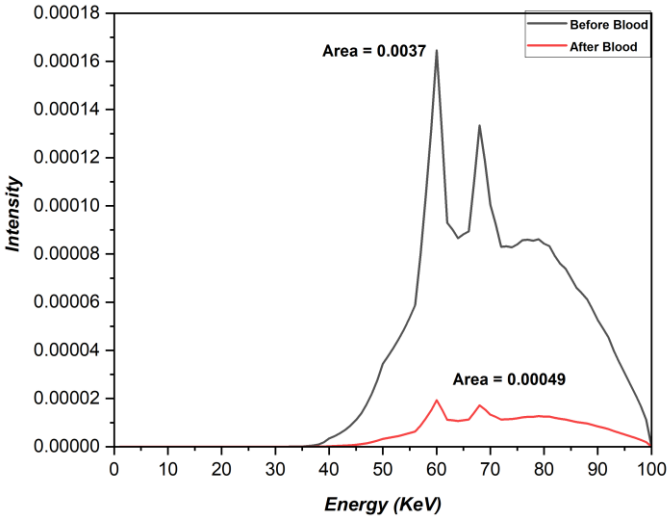

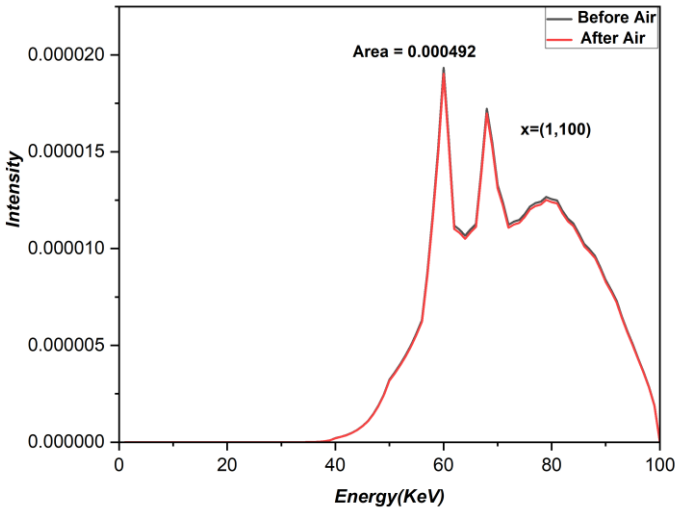

Fig.28 Relation between different intensity and energy after X-ray Attenuation

Conclusion

This study highlights significant advancements in gamma-ray detection and radiation protection using various high-performance detectors and theoretical calculations. The application of Cadmium Telluride (CdTe) detectors for calibration, alongside Bismuth Germanate (BGO) and Lanthanum Bromide ($LaBr_3$) scintillator detectors, enabled precise measurements and improved detection capabilities. The use of pixel detectors for alpha radiation assessment further diversified our approach. A key aspect of this research involved the theoretical determination of X-ray attenuation coefficients across different human body tissues, including tumors, fat, and muscle. By calculating these coefficients, we provided valuable insights into the variations in X-ray intensity before and after passing through different tissues. This theoretical approach is crucial for optimizing imaging accuracy and tailoring radiation doses to minimize exposure while maintaining diagnostic efficacy. Additionally, the incorporation of a monochromator to calculate the spacing distance of graphite atoms at different energy levels offered a deeper understanding of material interactions with radiation. This helped refine our methods and provided detailed spectra essential for various applications. Notably, our results indicate that the resolution of $LaBr_3$ detectors for Co-60 gamma emissions improves significantly with increased applied voltage. This enhancement in resolution underscores the importance of optimizing detector operating conditions to achieve superior performance in gamma spectroscopy.

Overall, this research demonstrates the critical role of advanced scientific tools in minimizing negative effects and unwanted exposure in medical imaging. By refining detector calibration, understanding tissue-specific radiation interactions, and employing theoretical approaches to X-ray attenuation, we can significantly enhance diagnostic accuracy and ensure better patient safety. These findings contribute to the ongoing development of more effective and safer radiation-based diagnostic and therapeutic techniques.

References

1. Persson, M., Wang, A., & Pelc, N. J. (2020). Detective quantum efficiency of photon-counting CdTe and Si detectors for computed tomography: a simulation study. Journal of Medical Imaging, 7(4), 1.
2. Si-PIN vs CdTe Comparison– Amptek – X-Ray Detectors and Electronics. (n.d.). Retrieved May 31, 2023
3. Schematic of a hybrid pixel detector with the sensor chip and the Download Scientific Diagram. (n.d.). Retrieved May 31, 2023
4. Poikela, T., Ballabriga, R., Buytaert, J., Llopart, X., Wong, W., Campbell, M., Wyllie, K., van Beuzekom, M., Schipper, J., Miryala, S., & Gromov, V. (2017). The VeloPix ASIC. Journal of Instrumentation, 12(1).
5. Knoll, G. F., Radiation detection and measurement, 4th Edition, Wiley (2010).
6. Martin J.E., Physics for Radiation Protection, WILEY-VCH Verlag GmbH & Co. KGaA, Weinheim (2013)
7. Knoll, G. F., Radiation detection and measurement, 4th Edition, Wiley (2010)

Acknowledgement

I would like to extend my sincere gratitude to my supervisor, S.A. Shakour, for his invaluable guidance, encouragement and unwavering support. throughout this project. his expertise and insights have been instrumental in the success of this research. I also wish to thank the JINR START Programme team for their hard work and collaboration. I am deeply grateful for the opportunity to embark on this research journey and gain extensive scientific experience. The knowledge and skills acquired during this project have significantly contributed to my professional and academic growth. I appreciate the constructive feedback and continuous support from my colleagues and mentors, which have been crucial in overcoming the challenges and achieving the goals of this study.